TAK1-binding protein 1 is a pseudophosphatase

Sarah H. CONNER*[1], Gursant KULAR*[1], Mark PEGGIE*[1], Sharon SHEPHERD†[1], Alexander W. SCHÜTTELKOPF†, Philip COHEN* and Daan M. F. VAN AALTEN†[2]

*MRC Protein Phosphorylation Unit, School of Life Sciences, University of Dundee, Dundee DD1 5EH, Scotland, U.K., and †Division of Biological Chemistry and Molecular Microbiology, School of Life Sciences, University of Dundee, Dundee DD1 5EH, Scotland, U.K.

TAB1 [TAK1 (transforming growth factor-β-activated kinase 1)-binding protein 1] is one of the regulatory subunits of TAK1, a protein kinase that lies at the head of three pro-inflammatory kinase cascades. In the current study we report the crystal structure of the N-terminal domain of TAB1. Surprisingly, TAB1 possesses a fold closely related to that of the PPM (Mg^{2+}- or Mn^{2+}-dependent protein phosphatase) family as demonstrated by the close structural similarity with protein phosphatase 2Cα. However, we were unable to detect any phosphatase activity for TAB1 using a phosphopeptide or *p*-nitrophenyl phosphate as substrate. Although the overall protein phosphatase 2Cα fold is conserved in TAB1, detailed structural analyses and mutagenesis studies show that several key residues required for dual metal-binding and catalysis are not present in TAB1, although binding of a single metal is supported by soaking experiments with manganese and isothermal titration calorimetry. Thus, it appears that TAB1 is a 'pseudophosphatase', possibly binding to and regulating accessibility of phosphorylated residues on substrates downstream of TAK1 or on the TAK1 complex itself.

Key words: protein phosphatase, transforming growth factor-β-activated kinase 1-binding protein 1 (TAB1), transforming growth factor-β-activated kinase 1 (TAK1), pro-inflammatory cytokine, X-ray crystallography.

INTRODUCTION

TAK1 (transforming growth factor-β-activated kinase 1) is activated when cells are stimulated with bacterial LPS (lipopolysaccharide) or the pro-inflammatory cytokines TNF (tumour necrosis factor) and IL-1 (interleukin-1). It plays a key role in switching on several pro-inflammatory signalling pathways, including those that activate the MAPKs (mitogen-activated protein kinases), termed p38α MAPK, JNK1/2 (c-Jun N-terminal kinase 1/2) and ERK1/2 (extracellular-signal-regulated kinase 1/2), as well as the transcription factor NFκB (nuclear factor κB) (Figure 1A) [1,2].

TAK1 is complexed to two other proteins in cells, namely TAB1 (TAK1-binding protein 1) and either TAB2 or the structurally related TAB3 [3]. The activation of TAK1 by LPS or IL-1 is thought to be triggered by the formation of Lys^{63}-linked polyubiquitinated TRAF6 (TNF-receptor-associated factor 6) and its interaction with the ring finger domains of TAB2 and TAB3 [4]. This induces phosphorylation of the activation loop of TAK1, resulting in its activation.

We have shown that the extent of activation of TAK1 in cells is limited by a feedback control mechanism in which p38α MAPK down-regulates TAK1 (Figure 1A) [3,5]. This is mediated by the p38α MAPK-catalysed phosphorylation of TAB1 at Ser^{423} and Thr^{431} [5] and/or by the phosphorylation of TAB2 and TAB3 at sites that have yet to be defined [3]. The feedback loop provides a mechanism for co-ordinating the degree of activation of several pro-inflammatory signalling pathways and has important implications for the development of anti-inflammatory drugs. Thus inhibitors of p38α MAPK show efficacy in animal models of rheumatoid arthritis [6] and a number of these compounds have entered human clinical trials. However, these inhibitors also cancel the feedback control of TAK1, causing the hyperactivation of JNK and a more rapid activation of NFκB [5]. This may underlie some of the side effects of these drugs, which have prevented them, thus far, from advancing to later stage clinical trials.

It has been noticed that the N-terminal region of TAB1 shares weak homology with PP2C (protein phosphatase 2C) [7], a member of the PPM (Mg^{2+} or Mn^{2+}-dependent protein phosphatase) family of protein serine/threonine phosphatases. In contrast, the C-terminal region contains a docking site for p38α MAPK (between residues 371 and 436) [5,8] and a TAK1-binding domain (which lies within the C-terminal 68 residues of TAB1) [9–11]. The three-dimensional structure of a chimaeric protein in which the TAK1 catalytic subunit is fused covalently to the C-terminal 36 residues of TAB1 has recently been reported [12] and interaction with this α-helical fragment of TAB1 is sufficient to activate the TAK1 catalytic subunit. In the current paper, we describe the three-dimensional structure of the N-terminal domain of TAB1 determined by X-ray crystallography. Strikingly, the structure of TAB1 resembles that of PP2C with the addition of an unusual 'stalk-like' domain. However, dramatic changes in the active-site residues are observed. These changes, which we probed by mutagenesis and phosphatase assays, imply that TAB1 is no longer able to bind the two metal ions required for catalysis by PP2C, suggesting that it is unlikely to possess any phosphatase activity. Potential functions for this unusual 'pseudophosphatase' are discussed in the light of these results.

EXPERIMENTAL

Tryptic digestion of full-length human TAB1

Full length TAB1 was amplified from pET21a TAB1 [5] with a GC Rich PCR System (Roche) using oligonucleotides GCGGATCCGCGGCGCAGAGGAGGAGCT and GCGCGGCCGCCTACGGTGCTGTCACCACGCTC. The product was

Abbreviations used: ERK1/2, extracellular-signal-regulated kinase 1/2; GST, glutathione S-transferase; IL-1, interleukin-1; IPTG, isopropyl β-D-thiogalactoside; ITC, isothermal titration microcalorimetry; JNK, c-Jun N-terminal protein kinase; LPS, lipopolysaccharide; MAPK, mitogen activated protein kinase; NFκB, nuclear factor κB; PP2C, protein phosphatase 2C; PPM, Mg^{2+}- or Mn^{2+}-dependent protein phosphatase; PTP, protein tyrosine phosphatase; rmsd, root mean square deviation; STYX, phosphoSerine, phosphoThreonine or phosphotYrosine interACTion protein; TAK1, transforming growth factor-β-activated kinase 1; TAB1, TAK1-binding protein 1; TNF, tumour necrosis factor.

[1] These authors contributed equally to this work.

[2] To whom correspondence should be addressed (email dava@davapc1.bioch.dundee.ac.uk).

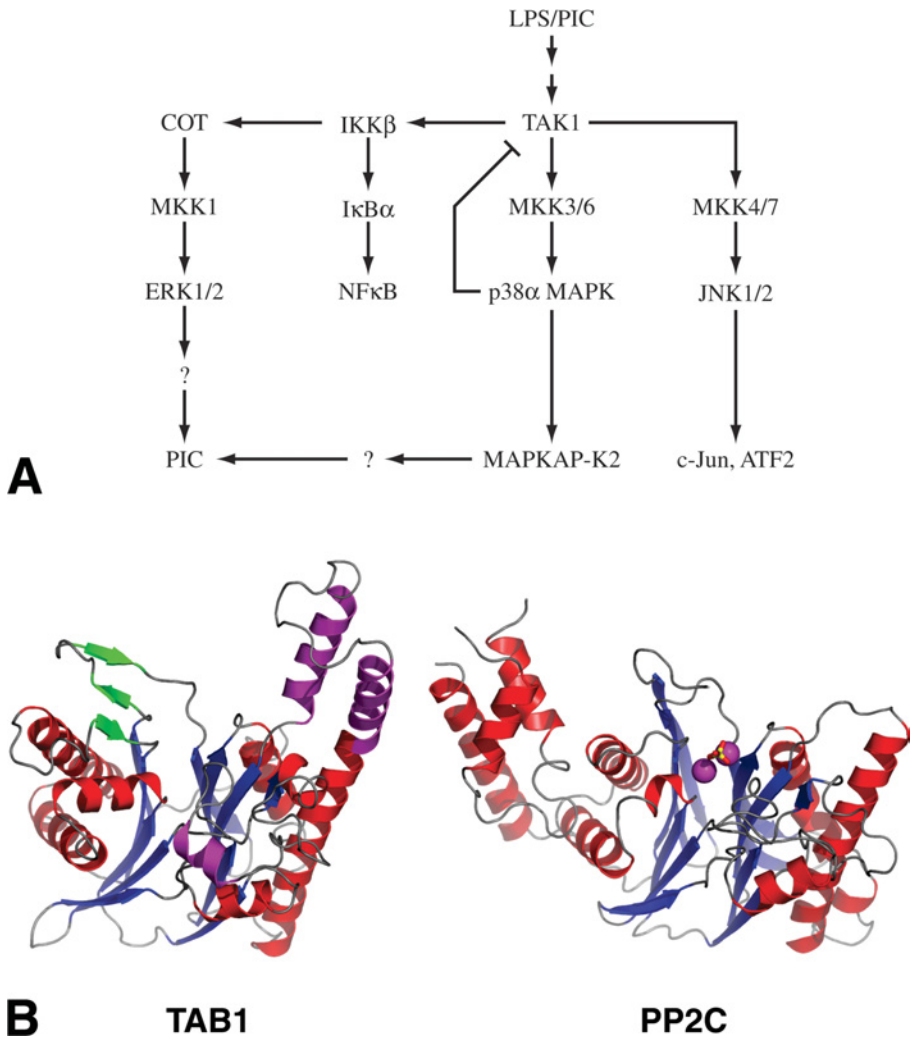

Figure 1 The TAK1 signalling pathway and comparison of the TAB1 and PP2C folds

(**A**) TAK1 is activated in response to LPS or pro-inflammatory cytokines (PIC), such as IL-1 and TNF. TAK1 then activates IKKβ (IκB kinase β) leading to activation of the transcription factor NFκB and the COT protein kinase (also called tumour progression locus 2, Tpl2). COT then activates MKK1 (MAPK kinase 1) and hence the extracellular-signal-regulated kinases ERK1 and ERK2. TAK1 also activates other MKKs and hence their downstream substrates, the p38α MAPK and JNK1/2. The substrates for p38α MAPK include the protein kinase MAPKAP-K2 (MAPK-activated protein kinase 2), whereas substrates for JNK include the transcription factors c-Jun and ATF2 (activating transcription factor 2). ERK1/2 and MAPKAP-K2 trigger the production of PIC, such as TNF, IL-6 and IL-8 (interleukin-8) by stabilizing the mRNAs, stimulating the translation and/or the secretion of these PIC. The substrates for ERK1/2 and MAPKAP-K2 that mediate these effects have not yet been fully defined. TAK1 is also subject to feedback regulation by p38α MAPK, providing a mechanism for limiting the activation of several pro-inflammatory pathways in a co-ordinated manner [5]. (**B**) The crystal structures of TAB1 and PP2Cα (PDB entry 1A6Q [20]) are shown in a ribbon presentation. Helices are coloured red and strands are coloured blue, with the exception of the TAB1 secondary structure elements that are not present in the PP2C structure (helices coloured magenta, strands coloured green). For the PP2C structure, the two active-site Mn^{2+} ions are shown as magenta spheres, together with the observed reaction product, phosphate (sticks).

sub-cloned into pFBHTb (Invitrogen) to produce pFBHTb TAB1, which was expressed in insect Sf21 cells to produce full-length His_6-tagged TAB1. After purification on nickel-nitrilotriacetate agarose and dialysis against 25 mM Tris/HCl (pH 7.5), 150 mM NaCl and 0.1 % (v/v) 2-mercaptoethanol, an aliquot (0.03 ml of a 0.8 mg/ml solution) was incubated for 30 min at 30 °C with 0–5 μg of trypsin. The trypsinized fragments were denatured in SDS containing 5 mM benzamidine and subjected to SDS/PAGE and staining with Coomassie Colloidal Blue. The major 43 kDa protein-staining fragment was subjected to Edman degradation to determine the N-terminal sequence, which showed that the fragment commenced at residue 7 of TAB1. The size of the fragment was estimated by calibrating the gel with marker proteins of known molecular mass, which indicated that the tryptic fragment was likely to terminate at Lys^{402}.

Cloning, expression and purification of TAB1[7–402]

DNA encoding human TAB1[7–402] was amplified using oligonucleotides GCGGATCCAGCTTGCTGCAGAGTGAGCAGC-AG and GCGGATCCTTACTTGCTGGTGCTCTGGGCGC. The resulting fragment was ligated into pCR2.1 (Invitrogen), sequenced, digested with BamH1 and subcloned into the same site in pGEX6P-1 to form pGEX6P-1 TAB1[7–402], which expresses a GST (glutathione S-transferase)–TAB1[7–402] fusion protein with a PreScission protease cleavage site between the GST and TAB1.

The human GST–TAB1[7–402] was expressed using *Escherichia coli* BL21 (DE3) cells. The cells were grown at 37 °C to an D_{600} of 0.6 in 5 litres of Luria–Bertani broth medium containing 100 μg/ml ampicillin, and then induced with 250 μM IPTG

Table 1 Details of data collection and structure refinement

Values in parentheses are for the highest resolution shell. All measured data were included in structure refinement. $KAu(CN)_2$, potassium aurocyanide. TAB1_high and TAB1_low refer to the high- and low-resolution native data sets collected.

	TAB1_high	TAB1_low	TAB1 + $KAu(CN)_2$	TAB1 + $MnCl_2$
Space group	P321	P321	P321	P321
Unit cell (Å)	$a = b = 141.97$, $c = 65.91$	$a = b = 143.41$, $c = 66.04$	$a = b = 143.42$, $c = 66.25$	$a = b = 141.26$, $c = 65.75$
Wavelength (Å)	1.03962	1.5418	1.03918	0.931
Resolution range (Å)	20–2.25 (2.33–2.25)	20–3.00 (3.11–3.00)	20–3.20 (3.31–3.20)	20–3.50 (3.62–3.50)
Observed reflections	151 048 (9864)	97 559 (9627)	135 233 (12 182)	74 851 (7828)
Unique reflections	35 816 (3001)	15 778 (1535)	12 874 (1243)	9779 (963)
Redundancy	4.2 (3.3)	6.2 (6.3)	10.5 (9.8)	7.7 (8.1)
$I/\sigma I$	13.6 (2.3)	12.9 (3.9)	9.5 (5.1)	12.1 (6.0)
Completeness (%)	98.0 (82.4)	99.7 (99.7)	99.6 (98.0)	100.0 (100.0)
R_{merge}	0.067 (0.467)	0.093 (0.542)	0.119 (0.466)	0.067 (0.428)
Protein residues	355			
Water molecules	83			
R, R_{free}	0.228, 0.236			
rmsd from ideal geometry				
Bonds (Å)	0.11			
Angles (°)	1.8			
B-factor rmsd (backbone bonds) (Å^2)	2.6			
⟨B⟩(Å^2)				
Protein	60.6			
Water	52.7			

(isopropyl β-D-thiogalactoside) and grown for 16 h at 26 °C. The cells were harvested by centrifugation at 3500 ***g*** for 20 min and then lysed by resuspension in 200 ml of lysis buffer [50 mM Tris/HCl (pH 7.5), 150 mM NaCl, 1 mM benzamidine, 1 mM PMSF and 0.1 % (v/v) 2-mercaptoethanol], containing DNase I (0.1 mg/ml) and lysozyme (1 mg/ml). After incubation on ice for 30 min and brief sonication, the lysate was cleared by centrifugation at 29 000 ***g*** for 30 min followed by incubation for 1 h at 4 °C with 7.5 ml of packed glutathione–Sepharose beads (Amersham Biosciences). The resin was washed with 200 ml of lysis buffer [50 mM Tris/HCl (pH 7.5), 500 mM NaCl and 0.1 % (v/v) 2-mercaptoethanol] and 500 ml of 50 mM Tris/HCl (pH 7.5), 300 mM NaCl and 0.1 % (v/v) 2-mercaptoethanol and then resuspended in 15 ml of 50 mM Tris/HCl (pH 7.5), 300 mM NaCl and 0.1 % (v/v) 2-mercaptoethanol. Cleavage of the GST–TAB1[7–402] fusion protein was then performed by incubation with 200 μg of GST-tagged PreScission protease for 16 h at 4 °C. The resulting supernatant was diluted in 50 mM Tris/HCl (pH 7.5) and 0.1 % (v/v) 2-mercaptoethanol, in order to decrease the NaCl to 50 mM. The protein was loaded on to a Mono-Q HP column (Amersham Biosciences) equilibrated in 50 mM Tris/HCl (pH 7.5) and 50 mM NaCl at a flow rate of 5 ml/min. The column was washed in the same buffer and TAB1 was eluted with a linear 120 ml salt gradient from 0–0.5 M NaCl in the same buffer. Fractions of 1.5 ml were collected. TAB1 that was eluted from Mono-Q at 175 mM NaCl was concentrated to 10 ml and loaded on to a 26/60 Superdex 200 gel-filtration column equilibrated in 50 mM Tris/HCl (pH 7.5), 300 mM NaCl and 1 mM dithiothreitol and the column was developed on an AKTA Explorer system (Amersham Biosciences). The TAB1 which coincided with the single peak of A_{280} absorbance, was pooled, concentrated to 10 mg/ml and used for crystallization.

Crystallization, data collection, structure solution and refinement

TAB1 was concentrated to 14.1 mg/ml and crystallized by vapour diffusion. A 1 μl aliquot of protein was mixed with 1 μl of mother liquor [100 mM Hepes (pH 7.5) and 1.5 M lithium sulphate] and 0.25 μl of 100 mM $BaCl_2$. Hexagonally-shaped crystals appeared within 3 days. Crystals were frozen in a nitrogen cryostream prior to data collection, using 100 mM Hepes (pH 7.5), 1.5 M lithium sulphate and 25 % (v/v) glycerol. Soaks with metals (potassium aurocyanide and $MnCl_2$) were performed by addition of 0.25 μl of a 4–10 mM stock directly to the drop with the crystals. 4 mM $MnCl_2$ was also part of the cryoprotecting solution used on the $MnCl_2$-soaked crystal. Synchrotron and rotating anode diffraction data were collected as shown in Table 1.

Experimental phases were obtained from a SIRAS experiment, with the gold derivative and a low-resolution (but more isomorphous) native data set, using HKL2MAP [13]. Two gold sites were located, and initial phases were calculated to 3.0 Å (1 Å = 0.1 nm) resolution. Solvent flattening and phase extension with the 2.25 Å native data set was then performed with DM [14], using a solvent content of 73 %, assuming one molecule per asymmetric unit. This yielded a readily interpretable electron density map, from which warpNtrace [15] was able to automatically build 320 residues. Further refinement (with CNS [16]) and model building (with O [17] and COOT [18]) then yielded the final model with the statistics shown in Table 1. Figures were made with PyMOL [19].

ITC (isothermal titration microcalorimetry)

Thermodynamic data for Mn^{2+} binding to TAB1[7–402] were determined by ITC using a VP-ITC instrument (Microcal). All experiments were carried out at 25 °C with a protein concentration of 0.181 mM and a concentration of the ligand ($MnCl_2$) of between 1.5 mM and 2.0 mM, both in 20 mM Tris/HCl (pH 7.5) and 100 mM NaCl. The binding curve was measured in triplicate and a full set of background corrections was obtained. Data integration, correction and analysis were carried out using Origin 5 (Microcal) with a single set of sites binding model.

Cloning, expression, purification and assay of wild-type and mutant PP2Cα

DNA encoding PP2Cα was amplified from pCW PP2C [20] using the GC Rich PCR System with oligonucleotides GCGGATCCATGGGAGCATTTTTAGACAAGCCAAAGATGG and

GCGCGGCCGCTTACCACATATCATCTGTTGATGTAGAGT-CAGTG. The product was ligated into pCR2.1 (Invitrogen), sequenced and then sub-cloned into the BamH1/Not1 sites of pGEX6P-1. H62Y, D239E and D282E single mutants were then made using the Stratagene QuickChange site-directed mutagenesis protocol. The wild-type and mutant GST–PP2C fusion proteins were expressed in *E. coli* (induced with 0.25 mM IPTG for 16 h at 26 °C), purified on glutathione–Sepharose and dialysed against 50 mM Tris/HCl (pH 7.5), 0.1 mM EGTA and 0.1 % (v/v) 2-mercaptoethanol. Aliquots were stored frozen at −20 °C at 1–5 mg/ml.

The PP2C preparations were assayed at 26 °C in 50 mM Tris/HCl (pH 7.5), 0.1 mM EGTA and 0.1 % (v/v) 2-mercaptoethanol at concentrations ranging from 0.01–0.1 mg/ml using 5 mM *p*-nitrophenyl phosphate (5 mM) as substrate in the presence of 2 mM $MnCl_2$ or 10 mM $MgCl_2$. The reactions (0.2 ml) were initiated with enzyme and initial velocities determined by monitoring the formation of *p*-nitrophenol from absorbance changes at 405 nm using a VersaMax microplate reader. PP2C preparations were also assayed at 26 °C using 1 mM of the synthetic phosphopeptide Arg–Arg–Ala–pThr–Val–Ala (where pThr is phosphothreonine) in the presence of either 2 mM $MnCl_2$ or 10 mM $MgCl_2$ [21]. The assays (0.025 ml) were stopped by the addition of 0.1 ml Malachite Green in 1 M HCl and, after incubation for 15 min, the phosphate released from the substrate was measured from the absorbance at 620 nm. Control experiments were carried out in which the PP2C was replaced by the buffer against which it was dialysed.

RESULTS AND DISCUSSION

Structure of the TAB1 N-terminal domain

Full-length TAB1 was overexpressed in *E. coli*, but failed to crystallize. Using limited proteolysis in combination with mass determination and N-terminal sequencing, a trypsin-resistant fragment was identified (residues 7–402), which was readily overexpressed in *E. coli* as a GST-fusion protein (25 mg/l bacterial culture). Affinity purification followed by cleavage with PreScission protease and further ion-exchange chromatography in the absence of divalent cations yielded pure protein (15 mg from 1 litre of bacterial culture), which was concentrated to 10 mg/ml and crystallized from lithium sulphate solutions. The crystals obtained were very fragile. Rotating anode and synchrotron diffraction data were collected on the native crystals (Table 1). Soaks with potassium aurocyanide yielded a suitable derivative for which a 10-fold redundant data set were collected. A SIRAS phasing strategy produced a good quality 2.25 Å electron density map that was used for automated and manual building, interspersed with refinement, yielding a final model with an *R*-factor of 0.228 ($R_{free} = 0.236$), with one TAB1 molecule in the asymmetric unit. TAB1 possesses an α/β fold, formed by two stacked five-stranded anti-parallel β-sheets, surrounded by α-helices (Figure 1B).

The structure of TAB1 is similar to PP2C

Potential similarity between TAB1 and previously solved protein structures was investigated with a DALI search [22]. Strikingly, the structure most similar to TAB1 is that of PP2Cα (PDB entry 1A6Q [20]), a metal-dependent protein serine/threonine phosphatase from the PPM family (Figure 1B). The three-dimensional structure of PP2Cα superimposes on TAB1 with an rmsd (root mean square deviation) of 1.8 Å on 236 equivalent Cα atoms (Figure 1B). With the exception of the N-terminal β-strand, the entire β-sandwich of PP2C is conserved in TAB1. Similarly, the helices immediately surrounding the β-sandwich are topologically conserved between PP2C and TAB1. However, the three-helical bundle that makes up the C-terminal domain of PP2C is absent in the TAB1 structure, as a result of the TAB1 construct boundaries established by limited proteolysis. A structure-based sequence alignment revealed weak amino acid sequence homology between PP2C and TAB1 (17 % identity; Figure 2A). Notably, three large (10–29 residues) insertions are seen in the TAB1 structure/sequence compared with PP2C. Two of these (36–45 and 340–354) form a three-stranded anti-parallel β-sheet displayed on the TAB1 surface (Figure 1 and Figure 2). In addition, a single 29 residue insertion, consisting of two α-helices, forms a stalk-like protrusion in TAB1 (Figure 1 and Figure 2). This stalk has a number of notable structural features. The two helices are amphipathic, with the hydrophobic faces interacting through small hydrophobic residues. Both basic and acidic side chains are displayed at the surface, six of which are involved in three salt bridges. The loop between the helices has an unusually high proline content (four out of fifteen residues; Figure 2A) and is ordered in the electron density map. Structural similarity searches with the stalk fragment did not reveal similar protruding features on other known protein structures.

The active site of PP2C is partially conserved in TAB1

Although TAB1 is topologically very similar to PP2C, the sequence conservation is low (Figure 2A). When this sequence conservation is mapped on to the TAB1 surface (Figure 2B), it becomes apparent that some of this sequence conservation locates to the area equivalent to the PP2C active site. PP2C possesses a highly negatively charged active-site cleft, which is important for tight binding of the two catalytically important Mn^{2+} ions (Figure 2C) [20]. The TAB1 surface also appears to be dominated by negative charges (Figure 2C), although no ions were observed in the TAB1 structure. The extra β-sheet and stalk in TAB1 produced a much deeper groove than that observed for the active site in the PP2C structure.

Direct comparison of the PP2C active-site with the equivalent region in TAB1 reveals a number of interesting similarities and differences. In PP2C, two Mn^{2+} ions are co-ordinated octahedrally through direct interactions with four aspartic acid residues, together with further co-ordination by protein-bound water molecules (Figure 3A). In TAB1 grown in the absence of Mn^{2+}, no such ions are observed, and the equivalent space is taken up by four water molecules. Furthermore, only two of the six side chains directly or indirectly involved in metal co-ordination in PP2C are identical in TAB1 (Glu^{50} and Asp^{51}; Figure 2A and Figure 3). The remaining four side chains have been substituted conservatively in TAB1 (Asn^{69}, Glu^{290}, Glu^{356} and Asp^{357}). Interestingly, the roles of several of these PP2C metal-binding residues have been investigated [23]. No significant effect on either turnover or substrate/metal binding was observed on mutation of Glu^{37} and Asp^{38}, equivalent to the two residues conserved within TAB1. However, mutation of the PP2C Asp^{60} to Asn, identical with the substitution seen in TAB1 (Asn^{69}), reduced k_{cat} by three orders of magnitude, together with a 40-fold increase in K_m for the metal. Similar deleterious effects on k_{cat} and K_m were seen for the PP2C D239N mutation. In the current study, we found that the mutation of Asp^{239} to the residue found in TAB1 (glutamatic acid) abolished PP2C activity (Table 2), suggesting that, although these substitutions in TAB1 are conservative, they greatly impair the ability of TAB1 to bind metals and perform catalysis.

The PP2C mutagenesis study also addressed the residues directly involved in catalysis [23]. PP2C is thought to hydrolyse the P–O bond through an acid/base catalytic mechanism, involving an activated water molecule [20,23]. Asp^{282} (Glu^{356} in TAB1) is

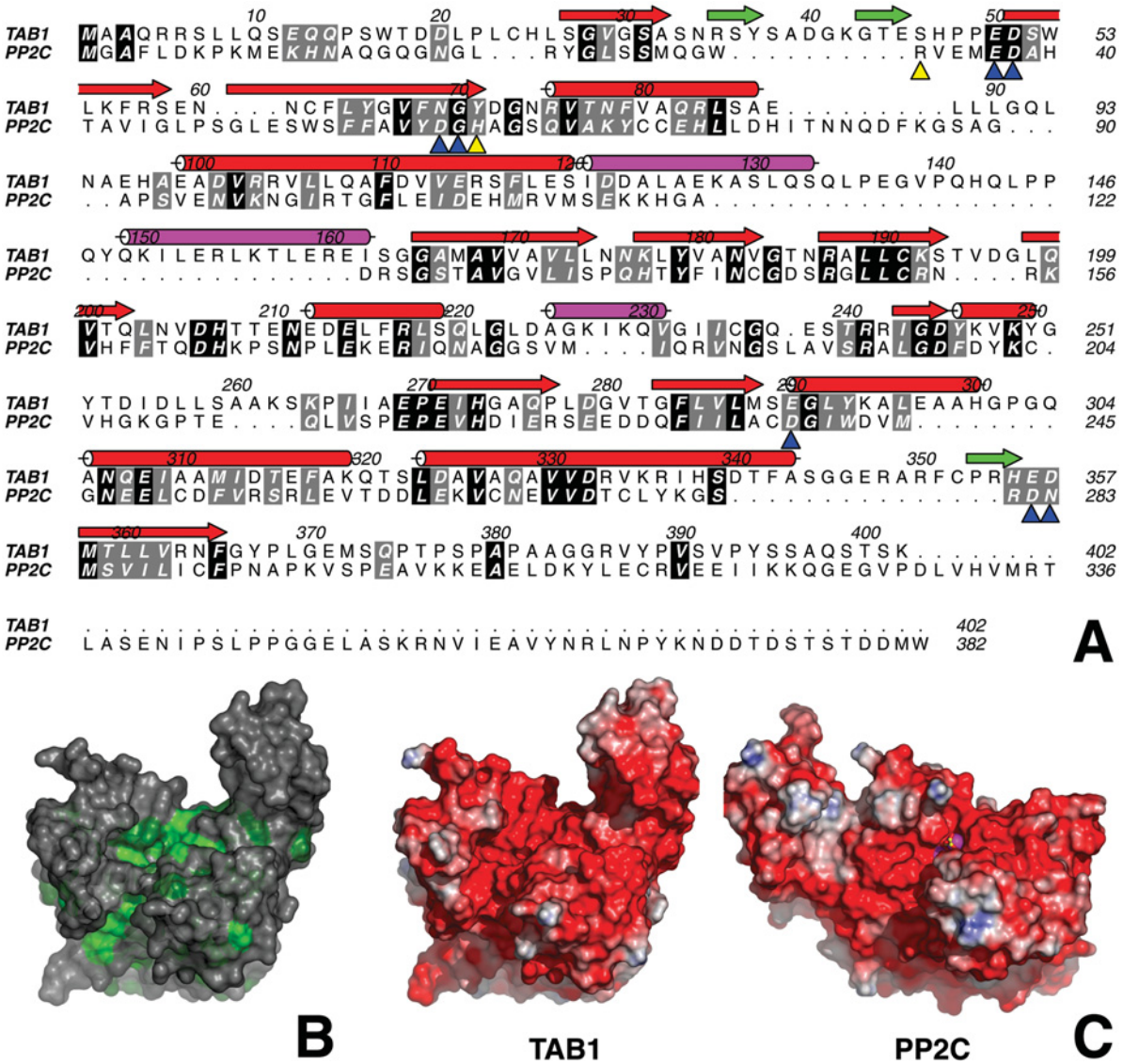

Figure 2 Structure-based sequence alignment of TAB1 and PP2C

(**A**) Structure-based sequence alignment of TAB1 and PP2C produced with ALINE (http://stein.bioch.dundee.ac.uk/~charlie/software/aline). TAB1 secondary structure elements are shown, using the same colour scheme as in Figure 1(**B**). PP2C residues that form direct or water-mediated interactions with the Mn^{2+} ions are indicated by blue triangles. Further residues thought to participate in catalysis/substrate binding are indicated by yellow triangles. (**B**) Sequence conservation between TAB1 and PP2C, mapped on to a surface representation of the TAB1 structure. Grey, not conserved; green, conserved; dark green, similar residues. (**C**) Comparison of electrostatic surface potential (calculated with APBS [27]) of TAB1 and PP2Cα, in the same orientation as Figure 1(**B**). Red is negatively charged (-5 *kT*), and blue is positively charged ($+5$ *kT*). For PP2Cα, the Mn^{2+} ions and the phosphate are also shown.

thought to be the catalytic base, abstracting a proton from a water molecule coordinated between the divalent metals. This water then performs nucleophilic attack on the phosphate, leading to a pentavalent transition state. Protonation by a catalytic acid, thought to be His^{62} (Tyr^{71} in TAB1), is believed to produce a phosphate-leaving group [23]. The negative charges of the substrate, transition state and product are thought to be stabilized through Arg^{33} (no equivalent in TAB1) and the mutation of this residue to alanine was found to decrease activity 20-fold [23]. Therefore, strikingly, none of these three catalytic residues are conserved in TAB1. We mutated Asp^{282} to the glutamic acid residue found in TAB1 and this caused an approximately 10- to 40-fold reduction in the activity of PP2C towards either the synthetic phosphopeptide RRATpVA or *p*-nitrophenyl phosphate (Table 2), similar to the 100-fold decrease observed by others towards *p*-nitrophenyl phosphate when Asp^{282} was mutated to asparagine [23]. Previous studies had also shown a 20-fold decrease in k_{cat} towards *p*-nitrophenyl phosphate when His^{62} was changed to glutamine and an 8-fold increase in the substrate K_m [23]. In agreement with this, we found that the mutation of His^{62} to the tyrosine residue present in TAB1 results in an approximately 100-fold decrease in the activity of PP2C towards the peptide substrate (Table 2). However, interestingly, towards the *p*-nitrophenyl phosphate, a 2-fold increase in activity was observed. More detailed kinetic analysis indicated that the H62Y mutation increased the k_{cat} from 0.076 min^{-1} in the wild-type enzyme to 0.152 min^{-1} in the mutant, the K_m for *p*-nitrophenyl phosphate being unchanged at 10 mM. These observations suggest that His^{62} may not be the catalytic acid, but is involved in stabilizing the leaving group required for the dephosphorylation of proteins

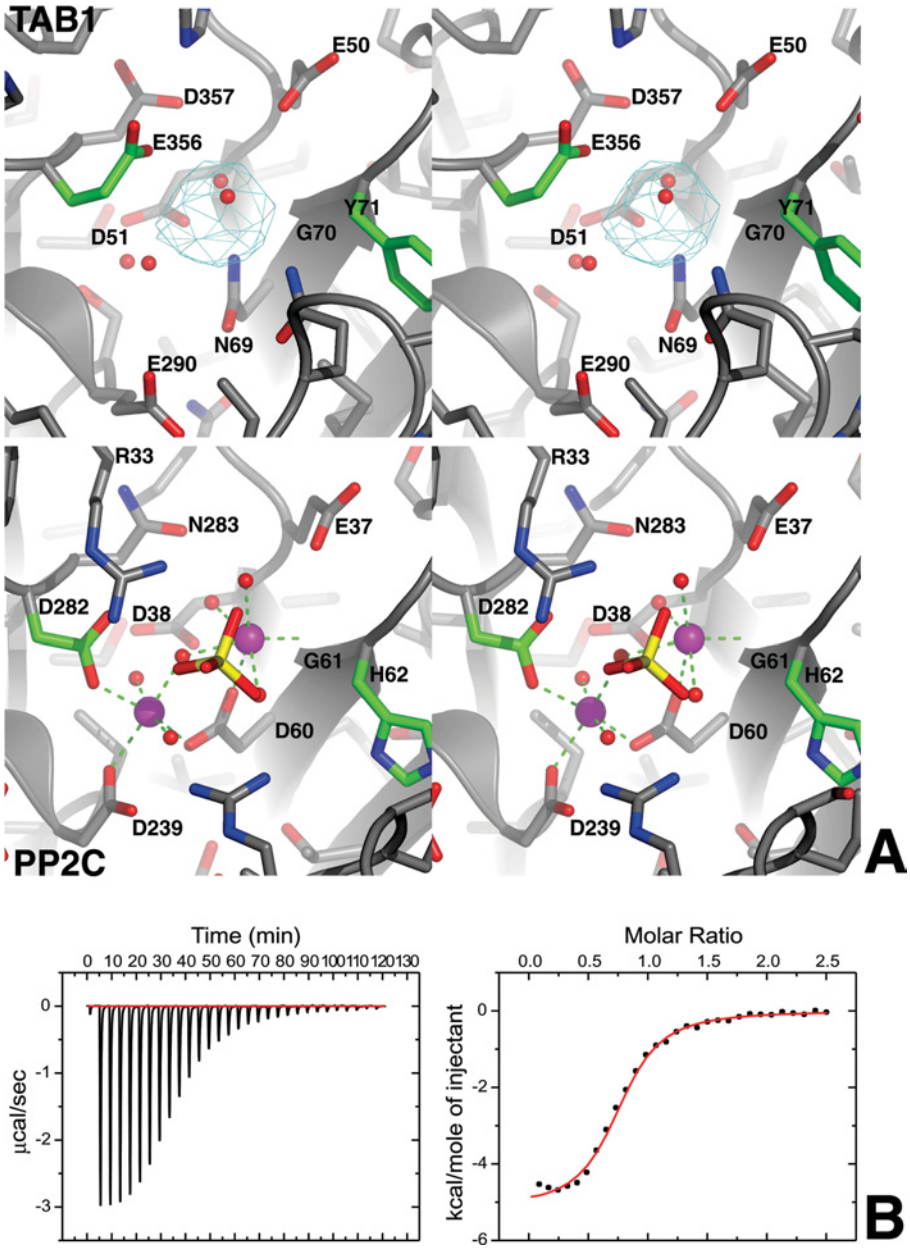

Figure 3 Comparison of the TAB1 and PP2C active sites, metal binding to TAB1

(**A**) Stereo views of the active-site structure of PP2C and the structurally equivalent region of TAB1. The protein backbones are shown as grey ribbons. Side chains are shown as sticks, those involved in metal binding or acid/base catalysis (green carbons) are labelled and also indicated in Figure 2(**A**). For PP2C, the Mn^{2+} ions and associated water molecules are shown, together with the phosphate product. For TAB1, water molecules occupying approximately equivalent positions to the water molecules/metals in the PP2C structure are shown, together with the 3.5 Å $F_o - F_c$ map (6σ) resulting from the manganese soak (Table 1). (**B**) ITC data for the binding of Mn^{2+} to TAB1. The differential power signal from a representative experiment is shown on the left; the integrated data (●) and fitted curve (solid line) for the same experiment are shown on the right.

and peptides, but not *p*-nitrophenyl phosphate. Furthermore, in a recently solved structure of a bacterial member of the PPM family, the equivalent residue is a methionine [24], suggesting that the identity of the catalytic acid in this family is as yet uncertain. In summary, these studies indicate that TAB1 is most unlikely to possess catalytic activity similar to PP2C.

The structural and mutagenesis studies described above suggest that TAB1 is not a catalytically active member of the PPM family of protein phosphatases. We therefore assayed TAB1 for protein phosphatase activity using either *p*-nitrophenyl phosphate or the peptide Arg–Arg–Ala–pThr–Val–Ala, which are two substrates employed commonly to measure PP2C [21]. No activity was detected towards either substrate in the presence of either 2 mM $MnCl_2$ or 10 mM $MgCl_2$, even after prolonged incubation at 0.1 mg/ml TAB1. Although PP2C was originally described as an Mg^{2+}-dependent enzyme, we also carried out experiments in the presence of Mn^{2+}, because some protein phosphatases that are inactive in the presence of Mg^{2+} do display activity in the presence of Mn^{2+}.

TAB1 binds a single Mn^{2+} ion

The crystal structure of PP2Cα was solved using bacterially expressed enzyme grown and purified in the presence of Mn^{2+}

Table 2 Activities of wild-type PP2Cα and TAB1 and mutant forms of PP2Cα towards two different substrates in the presence of magnesium or manganese ions

Activities towards the substrate RRATpVA (where Tp is phosphothreonine) are given as a percentage of that obtained with wild-type (WT) PP2Cα in the presence of 10 mM Mg^{2+}, whereas activities towards the substrate *p*-nitrophenyl phosphate (*p*NPP) are given as a percentage of that obtained with wild-type PP2Cα in the presence of 2 mM Mn^{2+}. The results are expressed as the means $\pm$ S.D. for at least three determinations for each phosphatase preparation. BLD, below the level of detection.

	RRATpVA		*p*NPP	
	10 mM Mg^{2+}	2 mM Mn^{2+}	10 mM Mg^{2+}	2 mM Mn^{2+}
WT PP2Cα	100 ± 4	34.4 ± 0.4	18.3 ± 2.9	100 ± 6
PP2Cα(H62Y)	0.69 ± 0.3	1.2 ± 0.1	54.5 ± 0.3	202 ± 14
PP2Cα(D282E)	0.07 ± 0.01	0.9 ± 0.9	$1.20 \pm$ I0.01	1.1 ± 0.1
PP2Cα(D239E)	BLD	BLD	< 0.01	BLD
WT TAB1	BLD	BLD	< 0.01	BLD

ions [20] and the published structure shows the presence of two manganese ions, despite the low metal affinity of PPM family members, with K_m values in the millimolar range [23]. Although no metal ions were observed in the TAB1 structure that we determined, this result was not definitive, because TAB1 was expressed in *E. coli* and purified in the absence of divalent cations. We therefore took three approaches to test the metal-binding ability of TAB1. First, TAB1 was purified in the presence of millimolar concentrations of $MnCl_2$ and crystallized under similar conditions. This appeared to consistently produce poorly diffracting crystals (e.g. diffraction around 4 Å resolution). Secondly, native TAB1 crystals were soaked in millimolar concentrations of $MnCl_2$. Although this also affected diffraction unfavourably, a 3.5 Å data set was collected. An $F_o - F_c$ difference electron-density map was calculated using phases calculated from the refined TAB1 model. Strikingly, a 13σ peak, presumably corresponding to a bound Mn^{2+} ion, was found in the active site (Figure 3A). This peak corresponds approximately to the position of the second Mn^{2+} ion in the PP2C structure, interacting with three of the protein ligands (the Gly^{70} backbone and the Glu^{50}–Asp^{51} side chains) that are conserved between TAB1 and PP2C (Figure 2 and Figure 3A).

Thirdly, to further investigate the affinity of the TAB1 active site for Mn^{2+} ions, ITC measurements were performed (Figure 3B). As expected for a highly charged ligand, the binding energy is dominated by a large negative enthalpic term [$\Delta H = (-19 \pm 2)$ kJ $\cdot$ mol^{-1}], even though entropy gains [$\Delta S = (35 \pm 7)$ J $\cdot$ $mol^{-1} \cdot K^{-1}$] make a significant contribution to the free energy of binding [$\Delta G = (-29.2 \pm 0.4)$ kJ $\cdot$ mol^{-1} and $k_d = 8 \pm 2$ μM]. With $n = 0.84 \pm 0.06$, the fitted number of binding sites per TAB1 molecule is close to 1.0, the value expected from the crystal structure. These data support the notion that TAB1 binds a single Mn^{2+} ion in its active site with low micromolar affinity, in agreement with the crystallographic data.

Conclusions

The evidence presented in the current paper indicates that, despite its overall structural similarity to PP2C, TAB1 is unlikely to be catalytically active as a protein phosphatase. Key residues required for the binding of divalent cations and catalysis are lacking and TAB1 has no detectable activity towards two substrates normally used to assay protein phosphatases of the PPM family. Nonetheless, calorimetric and structural data suggest that TAB1 binds a single divalent cation with a significantly higher affinity compared with the PP2C active site. These observations raise the question of the physiological roles of the pseudophosphatase domain of TAB1.

Yeast adenylate cyclase possesses a PP2C-like domain that, like TAB1, lacks several residues involved in PP2C catalytic activity [20]. Strikingly, mutation of one of the remaining putative metal co-ordinating residues (equivalent to Asp^{38} in PP2C and Asp^{51} in TAB1) causes a 50-fold reduction in the activation of adenylate cyclase by Ras–GTP. It has been hypothesized that, whereas the yeast adenylate cyclase does not possess PP2C-like phosphatase activity, the architecture of the active site could have been retained to provide a docking site for the γ-phosphate of GTP bound to Ras [20].

To the best of our knowledge, TAB1 is the first pseudophosphatase to be reported for the PPM family of protein phosphatases. For the PTP (protein tyrosine phosphatase) family, several such inactive catalytic domains, known as STYX (phosphoSerine, phosphoThreonine or phosphotYrosine interACTion proteins), have been reported [25]. These domains appear to have evolved from active PTPs, by mutation of the catalytic cysteine residue to a glycine residue, leading to proteins without phosphatase activity but with the retained ability to bind to phosphorylated proteins. The STYX proteins appear to act as anti-phosphatase proteins, preventing specific phosphorylated residues from becoming dephosphorylated [25].

It has been reported that PP2Cβ1 interacts with TAK1 and is involved in the dephosphorylation and inactivation of the TAK1 catalytic subunit [26]. It is therefore possible that the interaction of the C-terminus of TAB1 with TAK1 not only induces TAK1 catalytic activity, but also positions the pseudophosphatase domain of TAB1 in such a way as to interact with TAK1 in a similar manner to PP2Cβ1, sterically preventing PP2Cβ1 from dephosphorylating and inactivating TAK1. We further speculate that the p38α MAPK-catalysed phosphorylation of TAB1 induces a conformational change that facilitates the PP2Cβ1-catalysed inactivation of TAK1, which could underlie, at least in part, the feedback control of TAK1 activity by p38α MAPK [5].

We thank the European Synchrotron Radiation Facility, Grenoble, for the time at beamlines BM14 and ID14-3. D. vA. is supported by a Wellcome Trust Senior Research Fellowship, and P. C. by a Royal Society Research Professorship. We thank Helge Dorfmueller, Vincent Rao and Fabrizio Villa for their help with crystallization and data collection. We also thank the different services within the Division of Signal Transduction Therapy, School of Life Sciences, University of Dundee, Dundee for the production of many of the reagents used in this study, the DNA Sequencing Service (co-ordinated by Nick Helps) for sequencing the constructs and the Protein Production and Assay development team (co-ordinated by Hilary McLaughlan and James Hastie), for expression and purification of TAB1 and PP2C. We acknowledge the Medical Research Council, AstraZeneca, Boehringer–Ingelheim, GlaxoSmithKline, Merck and Co, Merck KGaA and Pfizer for financial support. The co-ordinates and structure factors have been deposited with the PDB (entry 2J40).

REFERENCES

1 Ninomiya-Tsuji, J., Kishimoto, K., Hiyama, A., Inoue, J., Cao, Z. D. and Matsumoto, K. (1999) The kinase TAK1 can activate the NIK-IκB as well as the MAP kinase cascade in the IL-1 signalling pathway. Nature **398**, 252–256

2 Lee, J., Mira-Arbibe, L. and Ulevitch, R. J. (2000) TAK1 regulates multiple protein kinase cascades activated by bacterial lipopolysaccharide. J. Leukocyte Biol. **68**, 909–915

3 Cheung, P. C. F., Nebreda, A. R. and Cohen, P. (2004) TAB3, a new binding partner of the protein kinase TAK1. Biochem. J. **378**, 27–34

4 Wang, C., Deng, L., Hong, M., Akkaraju, G. R., Inoue, J. and Chen, Z. J. J. (2001) TAK1 is a ubiquitin-dependent kinase of MKK and IKK. Nature **412**, 346–351

5 Cheung, P. C. F., Campbell, D. G., Nebreda, A. R. and Cohen, P. (2003) Feedback control of the protein kinase TAK1 by SAPK2α/p38α. EMBO J. **22**, 5793–5805

6 Lee, J. C., Laydon, J. T., McDonnell, P. C., Gallagher, T. F., Kumar, S., Green, D., McNulty, D., Blumenthal, M. J., Heys, J. R., Landvatter, S. W. et al. (1994) A protein-kinase involved in the regulation of inflammatory cytokine biosynthesis. Nature **372**, 739–746

7 Ge, B., Xiong, X., Jing, Q., Mosley, J. L., Filose, A., Bian, D., Huang, S. and Han, J. (2003) TAB1β (transforming growth factor-β-activated protein kinase 1-binding protein 1β), a novel splicing variant of TAB1 that interacts with p38α but not TAK1. J. Biol. Chem. **278**, 2286–2293
8 Ge, B., Gram, H., Di Padova, F., Huang, B., New, L., Ulevitch, R. J., Luo, Y. and Han, J. (2002) MAPKK-independent activation of p38α mediated by TAB1-dependent autophosphorylation of p38α. Science **295**, 1291–1294
9 Kishimoto, K., Matsumoto, K. and Ninomiya-Tsuji, J. (2000) TAK1 mitogen-activated protein kinase kinase kinase is activated by autophosphorylation within its activation loop. J. Biol. Chem. **275**, 7359–7364
10 Ono, K., Ohtomo, T., Sato, S., Sugamata, Y., Suzuki, M., Hisamoto, N., Ninomiya-Tsuji, J., Tsuchiya, M. and Matsumoto, K. (2001) An evolutionarily conserved motif in the TAB1 C-terminal region is necessary for interaction with and activation of TAK1 MAPKKK. J. Biol. Chem. **276**, 24396–24400
11 Sakurai, H., Miyoshi, H., Mizukami, J. and Sugita, T. (2000) Phosphorylation-dependent activation of TAK1 mitogen-activated protein kinase kinase kinase by TAB1. FEBS Lett. **474**, 141–145
12 Brown, K., Vial, S. C. M., Dedi, N., Long, J. M., Dunster, N. J. and Cheetham, G. M. T. (2005) Structural basis for the interaction of TAK1 kinase with its activating protein TAB1. J. Mol. Biol. **354**, 1013–1020
13 Pape, T. and Schneider, T. R. (2004) Hkl2map: a graphical user interface for macromolecular phasing with shelx programs. J. Appl. Cryst. **37**, 843–844
14 Cowtan, K. (1994) Dm: an automated procedure for phase improvement by density modification. Joint CCP4 and ESF-EACBM Newsletter on Protein Crystallography **31**, 34–38
15 Perrakis, A., Morris, R. and Lamzin, V. S. (1999) Automated protein model building combined with iterative structure refinement. Nat. Struct. Biol. **6**, 458–463
16 Brunger, A. T., Adams, P. D., Clore, G. M., Gros, P., Grosse-Kunstleve, R. W., Jiang, J.-S., Kuszewski, J., Nilges, M., Pannu, N. S., Read, R. J. et al. (1998) Crystallography and NMR system: a new software system for macromolecular structure determination. Acta Crystallogr. D, Biol. Crystallogr. **54**, 905–921
17 Jones, T. A., Zou, J. Y., Cowan, S. W. and Kjeldgaard, M. (1991) Improved methods for building protein models in electron density maps and the location of errors in these models. Acta Crystallogr. A **47**, 110–119
18 Emsley, P. and Cowtan, K. (2004) Coot: model-building tools for molecular graphics. Acta Crystallogr. D, Biol. Crystallogr. **60**, 2126–2132
19 DeLano, W. L. (2004) Use of PyMOl as a communications tool for molecular science. Abstr. Pap. Am. Chem. Soc. **228**, 030-CHED
20 Das, A. K., Helps, N. R., Cohen, P. T. W. and Barford, D. (1996) Crystal structure of the protein serine/threonine phosphatase 2C at 2.0 Å resolution. EMBO J. **15**, 6798–6809
21 Donella Deana, A., MacGowan, C. H., Cohen, P., Marchiori, F., Meyer, H. E. and Pinna, L. A. (1990) An investigation of the substrate specificity of protein phosphatase 2C using synthetic peptide substrates: comparison with protein phosphatase 2A. Biochim. Biophys. Acta **1051**, 199–202
22 Holm, L. and Sander, C. (1993) Protein structure comparison by alignment of distance matrices. J. Mol. Biol. **233**, 123–138
23 Jackson, M. D., Fjeld, C. C. and Denu, J. M. (2003) Probing the function of conserved residues in the serine/threonine phosphatase PP2Cα. Biochemistry **42**, 8513–8521
24 Pullen, K. E., Ng, H.-L., Sung, P.-Y., Good, M. C., Smith, S. M. and Alber, T. (2004) An alternate conformation and a third metal in PstP/Ppp, the M. tuberculosis PP2C-family Ser/Thr protein phosphatase. Structure **12**, 1947–1954
25 Wishart, M. J. and Dixon, J. E. (1998) Gathering STYX: phosphatase-like form predicts functions for unique protein-interaction domains. Trends Biochem. Sci. **23**, 301–306
26 Hanada, M., Ninomiya-Tsuji, J., Komaki, K., Ohnishi, M., Katsura, K., Kanamaru, R., Matsumoto, K. and Tamura, S. (2001) Regulation of the TAK1 signaling pathway by protein phosphatase 2C. J. Biol. Chem. **276**, 5753–5759
27 Baker, N. A., Sept, D., Joseph, S., Holst, M. J. and McCammon, J. A. (2001) Electrostatics of nanosystems: application to microtubules and the ribosome. Proc. Natl. Acad. Sci. U.S.A. **98**, 10037–10041

Received 14 July 2006; accepted 1 August 2006
Published as BJ Immediate Publication 1 August 2006, doi:10.1042/BJ20061077